Yin Yu
BioMfG Laboratory,
Center for Computer-Aided Design,
The University of Iowa,
Iowa City, IA, 52242;
Department of Biomedical Engineering,
The University of Iowa,
Iowa City, IA, 52242;
Department of Orthopaedics and Rehabilitation,
The University of Iowa,
Iowa City, IA, 52242

Yahui Zhang
BioMfG Laboratory,
Center for Computer-Aided Design,
The University of Iowa,
Iowa City, IA, 52242;
Department of Mechanical and
Industrial Engineering,
The University of Iowa,
Iowa City, IA, 52242

James A. Martin
Department of Orthopaedics and Rehabilitation,
The University of Iowa,
Iowa City, IA, 52242

Ibrahim T. Ozbolat[1]
BioMfG Laboratory,
Center for Computer-Aided Design,
The University of Iowa,
Iowa City, IA, 52242;
Department of Mechanical and
Industrial Engineering,
The University of Iowa,
Iowa City, IA, 52242
e-mail: ibrahim-ozbolat@uiowa.edu

Evaluation of Cell Viability and Functionality in Vessel-like Bioprintable Cell-Laden Tubular Channels

Organ printing is a novel concept recently introduced in developing artificial three-dimensional organs to bridge the gap between transplantation needs and organ shortage. One of the major challenges is inclusion of blood-vessellike channels between layers to support cell viability, postprinting functionality in terms of nutrient transport, and waste removal. In this research, we developed a novel and effective method to print tubular channels encapsulating cells in alginate to mimic the natural vascular system. An experimental investigation into the influence on cartilage progenitor cell (CPCs) survival, and the function of printing parameters during and after the printing process were presented. CPC functionality was evaluated by checking tissue-specific genetic marker expression and extracellular matrix production. Our results demonstrated the capability of direct fabrication of cell-laden tubular channels by our newly designed coaxial nozzle assembly and revealed that the bioprinting process could induce quantifiable cell death due to changes in dispensing pressure, coaxial nozzle geometry, and biomaterial concentration. Cells were able to recover during incubation, as well as to undergo differentiation with high-level cartilage-associated gene expression. These findings may not only help optimize our system but also can be applied to biomanufacturing of 3D functional cellular tissue engineering constructs for various organ systems. [DOI: 10.1115/1.4024575]

Keywords: bioprinting, cell-laden hydrogels, vascular constructs, tissue engineering

1 Introduction

For the past three decades, tissue engineering and regenerative medicine has emerged as a multidisciplinary field involving scientists, engineers, and physicians for the purpose of creating biological substitutes mimicking native tissue to replace damaged tissues or restore malfunctioning organs [1]. The traditional tissue engineering strategy is to seed cells onto scaffolds, which can then direct cell proliferation and differentiation into three-dimensional functioning tissue. Although significant success has been achieved in the past both in research and clinical applications of engineered tissues [2], challenges still exist toward organ fabrication in terms of the source of cells, optimization of scaffolds, approaches for functional three-dimensional organ formation [3,4], and most recently, large-scale manufacturing of living functional organ constructs for direct surgical implantation [5]. It is obvious that complex three-dimensional organs require more precise structures with vascular system integration, which cannot be fulfilled by traditional methods.

Recently, layer-by-layer additive manufacturing (AM) has been adapted to tissue engineering to direct the deposition of cells together with a hydrogel-base scaffold for 3D tissue and organ formation [6–8], which is also known as bioprinting. Bioprinting, or direct cell printing, is based on rapid prototyping (RP), using several different approaches. Inkjet printing [6,9–11], laser-based direct writing of cells [12–16], and extrusion-based cell-laden hydrogel deposition [17–19] are the most widely used technologies explored for this application. Computer-aided tissue fabrication offers great precision for the spatial placement of cells, rather than providing scaffold support alone [20], enabling direct manufacturing of living tissue parts and/or a functional living organ system. For example, AM-based direct deposition of tissue spheroids may lead to development of functional 3D organs [9,21]. One of the most critical challenges is the integration of a vascular network, without which the engineered 3D tissue or organ cannot receive sufficient nutrients and gas for its regeneration [22]. A number of approaches have been proposed and applied in fabricating vascular tissues with various cell-laden biomaterials. Xu and coworkers [23] designed and platform-assisted inkjet printing system to fabricate 3D zigzag cellular tubes vertically by fusion of sodium alginate droplet encapsulating 3T3 fibroblast cells. Ozawa et al. [24] applied an electrodeposition technique to deposit cell-laden alginate solution around Pt wire electrode and pulled out the electrode later to create hollow lumen of the vascular structure. Multiple cell types were deposited around the wire using that method. In addition, a scaffold-free approach was also developed by sequentially depositing tissue spheroids made purely from cells in cylindrical form, which later form a tubular structure by self-assembly of tissue spheroids [25]. From a single embryo to a sophisticated human body, cells have served as natural building

[1]Corresponding author.

Contributed by the Bioengineering Division of ASME for publication in the Journal of Biomechanical Engineering. Manuscript received November 7, 2012; final manuscript received May 1, 2013; accepted manuscript posted May 15, 2013; published online July 11, 2013. Assoc. Editor: Dror Seliktar.

blocks along the way of development. Studies have shown that cells are dynamically changing their growth pattern, spatial position, and differentiation under both mechanical and biochemical control of an extracellular matrix [22]. Any changes in these external cues may cause further intracellular downstream singling pathway activation, causing unpredictable cellular events. During the bioprinting process, cells receive different mechanical stimulation, which might affect intracellular structures and cell membrane integrity. As a result, it is critical to know whether cells can maintain their viability and/or desired phenotype after experiencing the bioprinting process. Some studies [13,26–28] have been performed to investigate bioprinting-process-induced cell injury. For syringe-based bioprinting, both nozzle diameter and material dispensing pressure were found to affect cell viability to some extent, immediately after bioprinting [26], and dispensing pressure has a more significant effect than nozzle diameter on cell viability. Cells were also observed to undergo apoptosis as well as necrosis after bioprinting [29]. In the literature, cellular structures have been evaluated for phenotypic alteration, and different tissue-specific differentiation has been achieved, like vascular tissue [30], cartilage [31], smooth muscle [32], etc. In this research, we developed a bioprinting system with a coaxial nozzle assembly for tubular channel fabrication. It is critical to know how the process parameters affect cell viability as well as phenotypes during cell-laden tubular channel bioprinting and postprinting incubation.

This work presents our recent study on the viability and functionality of cartilage progenitor cells (CPCs) [33], postencapsulation in sodium alginate, and printing through a pressure-assisted robotic bioprinting system. The bioprinting process dispenses cell-encapsulated sodium alginate through a coaxial nozzle system. Cells are inevitably subjected to different mechanical stimulus within the alginate solution. These stimuli associated with the bioprinting process might have an effect on cell viability following completion of the fabrication process and might also induce phenotypic alteration of cells in postprinting incubation. Four important parameters chosen in this study are nozzle diameter, alginate dispensing pressure, and cell seeding density and alginate concentration. Their effect on the viability and functionality of CPCs after the bioprinting process is reported. CPCs were used for a proof of concept in this study; various other cell types can be applied with the proposed system in future studies.

2 Materials and Methods

2.1 Materials. Prior to making a hydrogel solution, sodium alginate powder (Sigma Aldrich, United Kingdom) and calcium chloride powder (Sigma Aldrich, United Kingdom) were treated with ultraviolet (UV) light for sterilization three times for a 30-min cycle [34]. UV-sterilized sodium alginate was dissolved in deionized water to make 2%, 4%, and 6% (w/v) solutions. Solutions were mixed with a magnetic stirrer until homogeneity was reached. Similarly, the crosslinking solution was prepared by dissolving calcium chloride in ultrapurified water (Invitrogen™ Life Technologies, Carlsbad, CA) at 4% (w/v).

2.2 Cell Preparation. Bovine CPCs were isolated from as described in our previous study [33] and cultured at 37 °C in 5% CO_2 in Dulbecco's modified Eagle's medium (DMEM)/F12 (1:1) supplemented with 10% fetal bovine serum (Invitrogen™ Life Technologies, Carlsbad, CA), 50 μg/μl L-ascorbate, 100 μg/μl penicillin, 100 μg/ml streptomycin, and 2.5 μg/μl Fungizone. The culture medium was changed every other day. CPCs were passaged onto tissue culture dishes, and passage 1 cells were used for bioprinting. After harvesting, cells were gently mixed with the sodium alginate solution by repeated pipetting to get uniform distribution. Cell density varied from 2×10^6/ml to 8×10^6/ml in the alginate solution. CPCs were used in this study because their progenitor cells are sensitive to biochemical and mechanical changes, which has potential in cartilage tissue engineering applications.

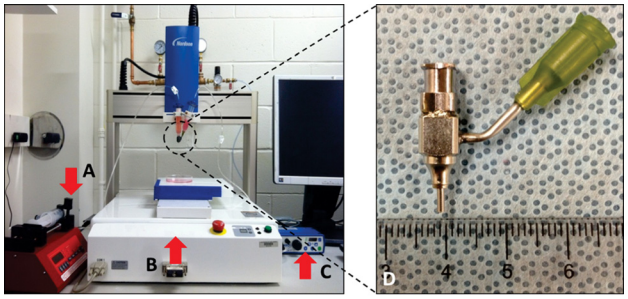

Fig. 1 Robotic bioprinting system and the coaxial nozzle assembly: single-arm robotic bioprinter with (*a*) a syringe pump, (*b*) a motion unit, (*c*) a pressure regulator, and (*d*) a physical coaxial nozzle system

2.3 Bioprinting Setup. An additive manufacturing-based robotic pressure-assisted bioprinting platform has been developed to do precise spatial deposition of cell-laden biomaterial as well as growth factors and biochemical compounds for tissue engineering constructs fabrication. The system used in this study consists of a single-arm robotic printer (EFD® Nordson, East Providence, RI) with a motion unit, a pressure regulator (EFD® Nordson), and a syringe pump (New Era Pump System Inc., Farmingdale, NY) (see Fig. 1), which enable printing cell-encapsulated biomaterials through a pressure-assisted computer-controlled system. A coaxial nozzle design (see Fig. 1(*d*)) was applied to fabricate tubular channels. Its opening diameter equals the difference between the inner diameter of the outer nozzle and the outer diameter of the inner nozzle. Viscous sodium alginate solution was extruded through the sheath section of the coaxial nozzle with low-pressure compressed air, while the calcium chloride solution was dispensed through the core section of the coaxial nozzle (see Fig. 2(*a*)). Crosslinking took place in the interface of the two materials, forming a tubular structure. Shear stress generated by this system is illustrated in Fig. 2(*b*).

2.4 Dispensing Rheology of Coaxial Flow. According to literature [35], the shear rate of a non-Newtonian flow through coaxial nozzle can be approximated as

$$\tau = \left(\frac{-\Delta P}{L}\right)\frac{R}{2}\left(\xi - \frac{\lambda^2}{\xi}\right) \tag{1}$$

In Eq. (1), Δp is the pressure change along the capillary, L is the capillary length of the coaxial nozzle, R is the inner radius of outer nozzle and $\xi = r/R$, and r is the radius of flow at a specific point inside the coaxial nozzle, with $r \in [\sigma R, R]$ (R is the inner radius of outer nozzle and σR equals the outer radius of the inner nozzle). λ is a constant locating the position of the maximum flow velocity and its value depends on the power-law flow behavior index (n) and σ ($\sigma = r_{\text{minimum}}/R$). The values of independent variables in Eq. (1) can be easily obtained except $-\Delta P/L$, which can be calculated as follows:

$$\frac{-\Delta P}{L} = \frac{Q}{\dfrac{n\pi R^3}{(3n+1)}\left(\dfrac{R}{4K}\right)^{1/n}\left\{(1-\lambda^2)^{(n+1)/n} - \sigma^{(n-1)/n}(\lambda^2-\sigma^2)^{(n+1)/n}\right\}}^{n} \tag{2}$$

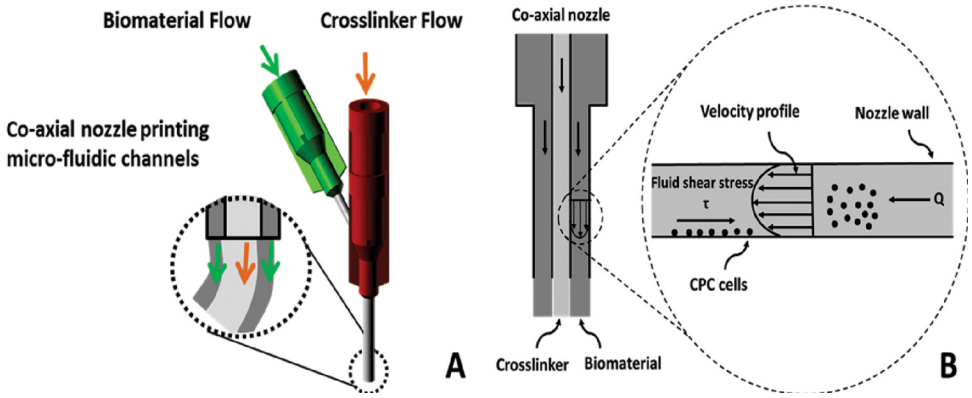

Fig. 2 Coaxial nozzle assembly and associated mechanical forces: (*a*) coaxial nozzle design for tubular channel manufacturing; (*b*) shear stress generated by coaxial nozzle system

In Eq. (2), K is the power-law consistency coefficient and Q is the volumetric flow rate.

2.5 Bioprinting Study. Cells were evenly distributed in alginate solution before bioprinting and were successfully encapsulated in tubular channels during the fabrication process. Cell viability assays were then performed to evaluate cell survival in response to varying bioprinting parameters. Prior to test-processing parameters, different cell density and sodium alginate concentrations were examined to find the optimal value in terms of high cell viability. Later, two printing process parameters were studied: a different-sized coaxial assembly for $I_{23G}O_{16G}$, $I_{26G}O_{16G}$ (I: inner nozzle; O: outer nozzle), and alginate dispensing pressures at 5 psi (35 kPa), 10 psi (69 kPa), and 20 psi (138 kPa). $I_{23G}O_{16G}$ consists of a 23 gauge (330 μm inner diameter, 650 μm outer diameter) inner nozzle and a 16 gauge outer nozzle (1190 μm inner diameter, 1460 μm outer diameter), while $I_{26G}O_{16G}$ has a 26 gauge inner nozzle (230 μm inner diameter, 457 μm outer diameter) and a 16 gauge outer nozzle. A calcium chloride crosslinking solution was dispensed at a constant rate for 2 ml/min in all experiments. Three samples were used for each experimental group ($n = 3$). Different cell densities were first used in a viability study for a single nozzle (16 G) to determine the optimal number to be used in later study. Direct crosslinking of the hanging alginate droplet on the nozzle tips was used as the control for all groups. Five to fifteen centimeters of printed tubular cell-laden channels were collected for each sample. Immediately after printing, each sample was kept in Hanks Balanced Salt Solution (HBSS) (Invitrogen™ Life Technologies, Carlsbad, CA) supplemented with 4% (w/v) calcium chloride for maintained crosslinking. Samples were washed with HBSS supplemented with 100 U/ml penicillin, 100 μg/ml streptomycin, and 2.5 μg/ml Fungizone for sterilization before incubation in cell culture media. Cell viability was evaluated at three incremental time points: 12 h, 24 h, and 72 h, for exactly the same samples in each group throughout the time course.

Postprinting cell functionality study was presented to examine bioprinting-induced cell phenotypic change. Longer samples (<50 cm) printed at optimal cell density were subjected to two weeks culture in DMEM-based media. For the control group, the same number of printed samples was dissolved in cell releasing buffer (55 mM sodium citrate, 30 mM ethylenediamine tetraacetic acid (EDTA), 0.15 M NaCl) after complete crosslinking in HBSS, following consequent plating of CPCs for monolayer culture instead of 3D tubular channel encapsulation. Quantitative reverse transcriptase polymerase chain reaction (RT-PCR) was used to check cartilage-associated genetic marker expression.

2.6 Cell Viability Assay. Calcein acetoxymethylester (calcein AM) and ethidiumhomodimer-2 (Invitrogen™ Life Technologies, Carlsbad, CA), at a concentration of 1.0 mM each, were used. Calcein AM labels living cells with bright green fluorescent. Ethidium homodimer is a red fluorophore that stains nonviable cells but cannot penetrate living cells. Each sample was washed with HBSS before live/dead staining. After 30-min incubation, samples were imaged using an Olympus FluoViewTM FV1000 laser scanning confocal microscope (LSCM) (Olympus NDT Inc., MA). Z-axis projections were assembled from images of each sample from surface to bottom with a depth of 1000 μm at 20-μm intervals. ImageJ software (National Institutes of Health, Bethesda, MD) was used for automated counting of red- and green-stained CPCs in z-axis projections, and percentages of viable cells were calculated. The percentage of viable cells for each experimental group was calculated by averaging the values of three different samples.

2.7 Cell Functionality Evaluation. Encapsulated CPCs were then released from cellular channels by dissolving them in dissolving buffer (55 mM sodium citrate, 30 mM EDTA, 0.15 M NaCl). Cells were centrifuged and washed twice in a phosphate buffer saline (PBS) (Invitrogen™ Life Technologies, Carlsbad, CA). Then the pellets were homogenized in TRIzol® reagent (Invitrogen™ Life Technologies, Carlsbad, CA), and total RNA was extracted using the RNeasy Mini Kit (QIAGEN, Valencia, CA) according to the manufacturer's instructions. Cartilage-specific gene expression (collagen type II, aggrecan, and Sox-9) was measured by real-time PCR in monolayer cultured CPCs and alginate encapsulated CPCs. Collagen type II is the basis for articular cartilage, and collagen type II gene is a marker related to chondrocyte phenotype and function. Aggrecan is a protein that in humans is encoded by the ACAN gene, which is an integral part of the extracellular matrix in cartilage tissue. Sox-9 is a transcription factor related to chondrogenic differentiation, which is the main function of CPCs. Primers were purchased from Integrated DNA Technologies (Coralville, IA).

2.8 Statistical Analysis. The statistical significance of experimental data was determined by two-way analysis of variance (ANOVA) for the dispensing pressure and nozzle diameter studies. One-way ANOVA was used for the cell density and alginate concentration studies, respectively. The pairwise test was combined with the Tukey post hoc test at a significance level of less than 0.05 ($p < 0.05$) using SPSS software.

3 Results

3.1 Bioprinted Cell-Laden Tubular Channels. Fabrication was performed using 4% alginate solution with a dispensing rate of 0.2 ml/min, and 4% crosslinker solution was dispensed at

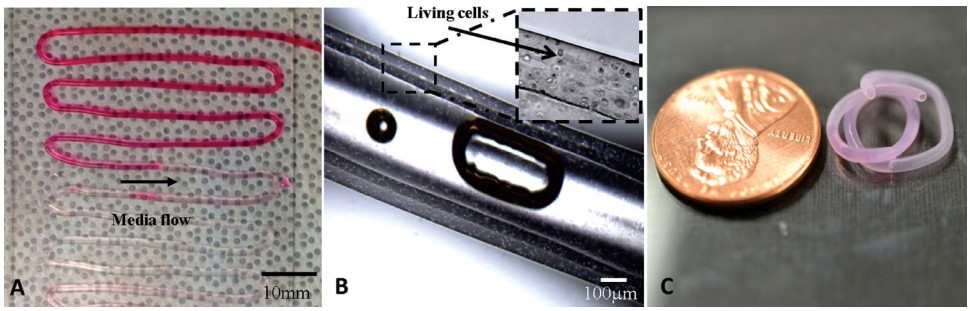

Fig. 3 Bioprinted cell-laden tubular constructs: (*a*) tubular channels were printed into zigzag orientation with perfused cell-type media, (*b*) bubble inclusion in tubular center demonstrating its hollow feature and microscopy images showing cell encapsulation in the wall of cellular channels with relatively uniform distribution of cells, and (*c*) an 1 week cultured cell-laden tubular channel showing promising mechanical and structural integrity

1.5 ml/min for gelation purposes as described in our previous study [36]. The average inner and outer diameters of the fabricated tubular channels were $135 \pm 13\,\mu$m and $309 \pm 22\,\mu$m, respectively. Printed structures were then examined under a Motic® BA310 digital microscope (Motic in North America, Canada). Pumping of food dye solution assisted by a syringe pump was performed on the printed tubular channel to confirm its media transportation ability. As presented in Fig. 3, tubular channels were successfully manufactured by coaxial nozzle design assisted by a bioprinter with continuous uniform structural integrity. Perfusion of oxygenized cell media without any swirling or leakage through a >10 cm long channel showed their ability to support media transportation at flow rate of 30 ml/min. Sufficient structural integrity was maintained during 3 h perfusion demonstrated its mechanical strength (see Fig. 3(*a*)). Experiments showed that tubular channels (7 cm in length), which have been soaked in 0.5% calcium chloride solution for 5 h after fabrication, had 5.65 ± 1.78 kPa maximum tensile stress with 5.91 ± 1.12 kPa Young's modulus. Intentional bubble inclusion clearly illustrated the hollow feature of the printed structure, and cells were

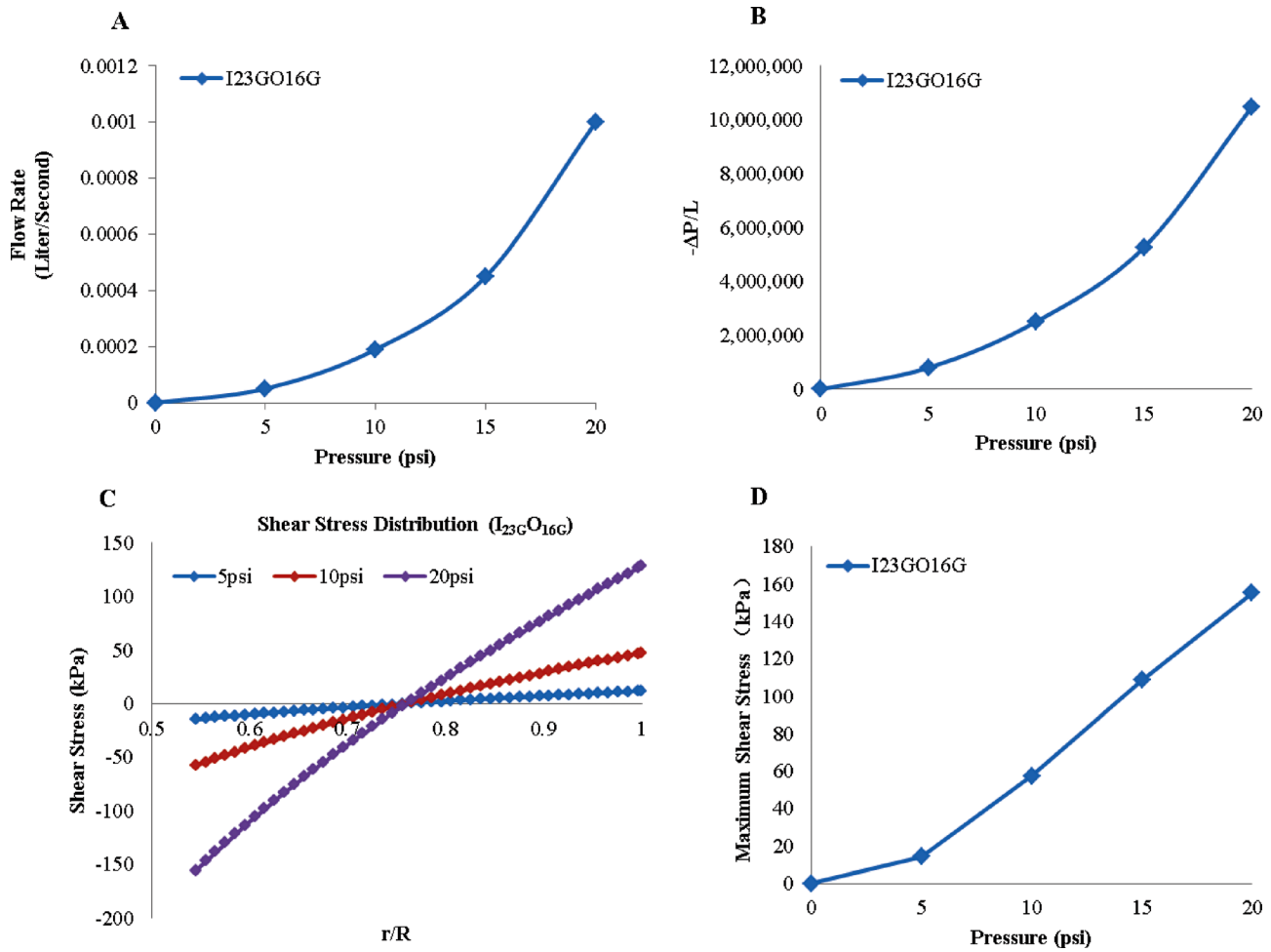

Fig. 4 Dispensing rheology ($I_{23G}O_{16G}$): (*a*) effect of alginate pressure rate on volume flow rate of 4% alginate solution, (*b*) effect of pressure rate on $-\Delta P/L$, (*c*) shear stress distribution in coaxial nozzles, and (*d*) maximum shear stress with varying alginate dispensing pressure

individually encapsulated and uniformly distributed in sodium alginate, forming a cellular wall of printed tubular structures (see Fig. 3(*b*)). Cell-laden tubular channels were able to maintain their morphology as well as hollow feature after 7 days incubation (see Fig. 3(*c*)).

3.2 Dispensing Rheology of Coaxial Flow. In order to calculate the shear stress, the value of $-\Delta P/L$ was calculated using Eq. (2), where $K = 14{,}960$ and $n = 0.86$ for 4% alginate [37]. The volumetric flow rate was obtained from experimental measurements and plotted in Fig. 4(*a*) and $-\Delta P/L$ is presented in Fig. 4(*b*) that was used in Eq. (1) to calculate the shear stress. The shear stress distribution in coaxial nozzles with 5 psi (35 kPa), 10 psi (69 kPa), and 20 psi (138 kPa) alginate dispensing pressures is demonstrated in Fig. 4(*c*). As depicted from the figure, shear stress reaches its maximum value on the outer surface of the inner nozzle. Then, the shear stress diminishes as r increases and vanishes at the inflection point somewhere around the middle point of the space between nozzles. The inflection point does not necessarily locate in the middle of the space between nozzles, however; its location depends on the value of λ. After the inflection point, the shear stress changes direction and increases as the r increases. This result is consistent with the observation in Fig. 6, in which most dead cells were observed on tubular channels walls, particularly more dead cells were observed on the inner wall than the outer wall. Figure 4(*d*) shows maximum shear stress value under various dispensing pressures. Maximum shear stress increases as the alginate dispensing pressure increase. This explained why cell viability significantly decreases with increased alginate dispensing pressure.

3.3 Effect of Cell Density and Sodium Alginate Concentration on Postprinting Viability. The first experiment was conducted to assess the effect of cell density in alginate solution and alginate concentration on cell viability in order to determine the optimal values for later studies. The three cell seeding densities used are 2×10^6/ml, 4×10^6/ml, and 8×10^6/ml in 2%, 4%, and 6% (w/v) alginate solution was printed through an 18 G single nozzle, with an inner diameter of 1.19 mm. Each data point was an average of three representative live/dead confocal images from three samples in each group. For each cell density, the dispensing pressure was studied at 5 psi (35 kPa), 10 psi (69 kPa), and 20 psi (138 kPa). Twelve hours postprinting and before cell proliferation, live/dead cell staining was carried out, and images were quantitatively analyzed by Image J. As shown in Fig. 5(*a*), although decreased cell viability was observed with increasing alginate dispensing pressure, there was no significant difference in the viability of different cell densities at the same pressure, with the highest average around 72% at 5 psi (35 kPa). However, cell viability decreased with increasing alginate concentration (see Fig. 5(*b*)). The highest cell viability was 89% for 2% alginate, with a significant drop (31%) for 6% alginate. Since 4% alginate offered acceptable cell viability at 68% and reasonable structural integrity [36] of the printed channels, a 4% alginate solution and 2×10^6 cells/ml will be used in later studies.

3.4. Effect of Coaxial Nozzle Size and Alginate Dispensing Pressure on Cell Viability. To examine the effect of the bioprinting process on cell viability, experimental studies were designed to assess the effect of the nozzle size and alginate dispensing pressure on the viability of cells. The viability was calculated by averaging three representative live/dead confocal images for each sample. Analysis was first performed by segregating the samples into two experimental groups according to different coaxial nozzle assemblies: $I_{23G}O_{16G}$ (outside diameter (OD) = 550 μm) and $I_{26G}O_{16G}$ (OD = 730 μm). For each coaxial nozzle, various dispensing pressures were studied at 5 psi (35 kPa), 10 psi (69 kPa), and 20 psi (138 kPa). A z-axis stack of confocal images is shown in Fig. 6, demonstrating live/dead cells, their relative ratios, and their distribution in printed cellular channels (the first 10 images from the top surface were eliminated to show the hollow feature of the printed structures). Quantitative viability assays are presented in Fig. 7 to show the effects of alginate dispensing pressure and coaxial nozzle size.

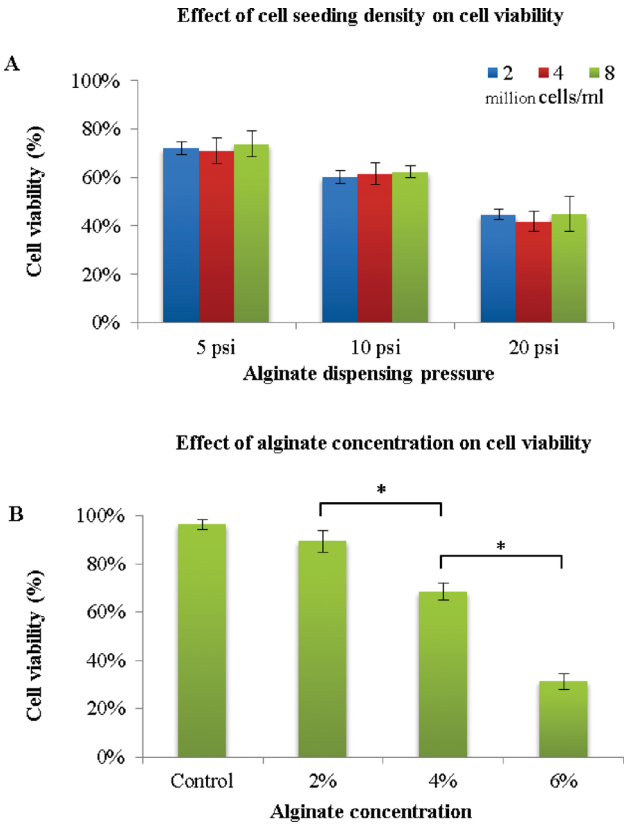

Fig. 5 Quantitative cell viability for various cell densities and alginate concentrations: (*a*) effect of cell density on cell viability at different alginate dispensing pressures, (*b*) effect of sodium alginate concentration on cell viability at 5 psi (35 kPa) with cell density of 2×10^6 cells/ml (data are mean ± SD; $p < 0.05$)

Based on the figures, it is obvious that cell viability varies with varying alginate dispensing pressures and different coaxial nozzle sizes. Printed cell viability decreases with increasing alginate dispensing pressure, and higher viability was observed in a coaxial nozzle of a larger size ($I_{26G}O_{16G}$). Changing the alginate dispensing pressure resulted in a significant difference in cell viability among experimental groups over the time course, especially at early time points. For the nozzle $I_{23G}O_{16G}$ (550 μm), a significant

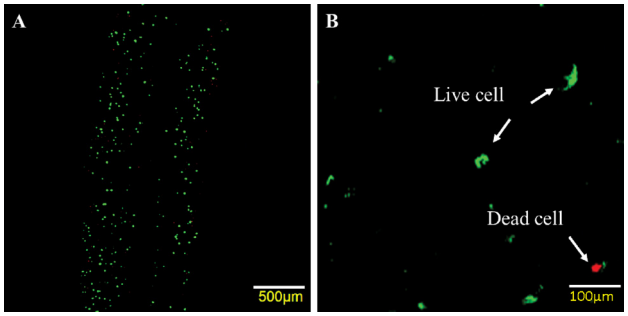

Fig. 6 Laser confocal imaging for live/dead staining of the printed structure at 5 psi (35 kPa) with $I_{23G}O_{16G}$ nozzle: CPCs labeled with calcein AM and ethidium homodimer after cell encapsulation and imaged with confocal laser scanning microscope: (*a*) quantifiable dead cells were present, while most of cells were viable; (*b*) zoom-in image shows live and dead cells with fluorescence green and red, respectively

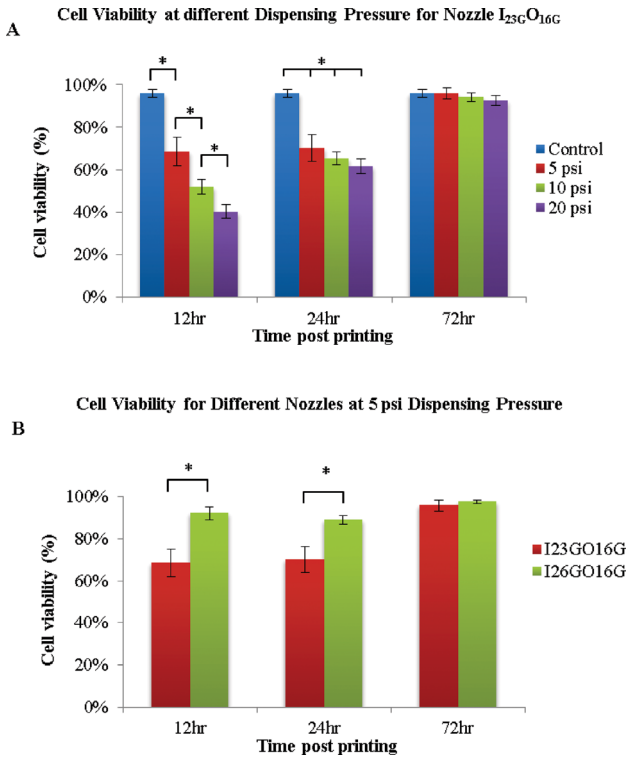

Fig. 7 Effect of bioprinting parameters on cell viability for 72 hr postbioprinting: (*a*) effect of alginate dispensing pressure (psi) on cell viability, (*b*) cell viability for different-sized coaxial nozzle assemblies (data are mean ± SD; $p < 0.05$)

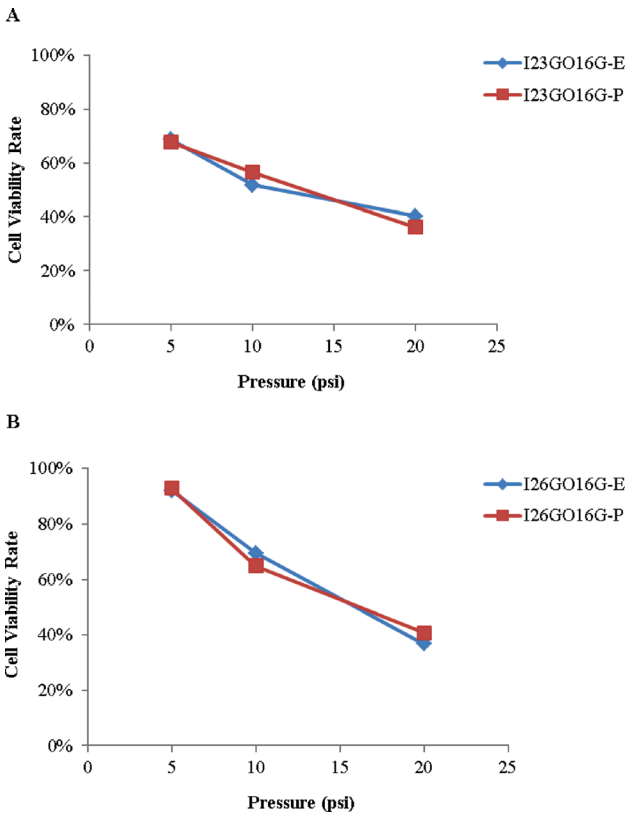

Fig. 8 Experimental and predicted cell viability (E: experimental; P: predicted): (*a*) for nozzle $I_{23G}O_{16G}$; (*b*) for nozzle $I_{26G}O_{16G}$

decrease in cell viability was observed in the bioprinted tubular structures compared with the control group shortly after printing (12 h) and at the 24 h time point as well (see Fig. 7(*a*)). The cell viabilities of the experimental groups at 12 h for varying alginate dispensing pressure (5 psi (35 kPa), 10 psi (69 kPa), and 20 psi (138 kPa)) were 68%, 51.75%, and 40%, respectively. For a given representative alginate dispensing pressure (10 psi (69 kPa)), a small nozzle $I_{23G}O_{16G}$ (550 μm) resulted in a statistically significant drop in cell viability between the experimental group and the normal control group within 12 h postprinting and at the 24 h time point (see Fig. 7(*b*)), while there was no significant change in cell viability in channels printed by the larger nozzle, $I_{26G}O_{16G}$. The cell viabilities of the control group were 95%, and the experimental groups with nozzles size of 730 μm and 550 μm were, 92% and 68%, respectively.

An empirical mathematical model was derived to predict cell viability V (%) at 12 h. Two variables, spaces between nozzles (X_1-cm) and alginate dispensing pressure (X_2-psi), are considered as independent prediction factors. The predicted cell viability and experimental cell viability are plotted in Fig. 8 for both nozzle $I_{23G}O_{16G}$ and $I_{26G}O_{16G}$. According to Fig. 8, the predicted cell viability percentage is relatively close to the experimental results. The average percentage of error of the prediction model is small (6.43%).

$$V = -213.68X_1^2 + 33.61X_1 - 0.07X_2 - 0.2 \quad (3)$$

3.5 Postprinting Cell Recovery During Incubation. We also elicited that cell viability increased during incubation from 12 h to 72 h postprinting. From confocal imaging, the ratio of red fluorescent dead cells decreases, while green fluorescent live cells increases (see Fig. 9).

Quantitative analysis of cell viability at different time points was also performed. Figure 10 showed an increasing trend of cell viability in the printed structure with the $I_{26G}O_{16G}$ coaxial nozzle. For all dispensing pressures (i.e., 5 psi (35 kPa), 10 psi (69 kPa), and 20 psi (138 kPa)), a significant increase in cell viability (97%, 97%, and 98%, respectively) was observed at the 72 h time point. Cell viability in all groups was approaching or exceeding the control group at the end of 72 h incubation. For the 5 psi (35 kPa) and 10 psi (69 kPa) dispensing pressures, cell viability did not increase significantly over the 24 h period, but noticeable increases were observed at the 72 h time point from 89% to 97% and from 69% to 97%, respectively. For the 20 psi (138 kPa) dispensing pressure, there was a remarkable increase in cell viability at both the 24 h (63%) and 72 h (98%) time point compared with the 12 h (36%) time point.

3.6 Postprinting Cell Functionality. As cartilage progenitor cells are tissue-specific stem cells of cartilage tissue, they should have the potential to undergo chondrogenic differentiation. When differentiated, their main function is to produce extracellular matrix (ECM) of articular cartilage. Gene expression analysis is sufficient to check cell functionality based on their genetic markers for specific ECM proteins. Gene expression analysis revealed relatively higher expression of cartilage-specific marker genes in CPCs encapsulated in hollow fibers versus monolayer cultured CPCs. In real-time PCR analysis, collagen type II (COL-2), Sox-9 showed over a twofold change, which indicated that CPCs were better differentiated towards chondrogenic lineage, making cartilage-specific protein to serve as extracellular matrix. Aggrecan genes (ACAN) were upregulated to over 12-fold in bioprinted structures, which further supports that the tubular alginate channel is an ideal environment for CPCs to differentiate and carry out their cartilage-producing function (see Fig. 11).

4 Discussion

In this study, the proposed bioprinting system together with the coaxial nozzle assembly successfully generates cellular vessellike tubular cell-laden channels with media transportation capability.

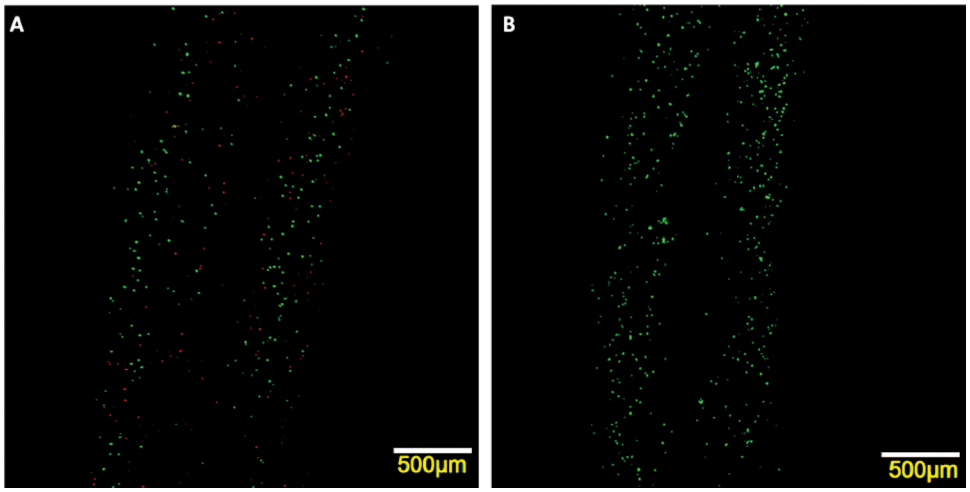

Fig. 9 Laser confocal imaging for live/dead staining of the same sample at different time points: (*a*) 12 h postprinting, massive cell death (red fluorescent) was observed all over the printed structure; (*b*) after 72 h incubation, a few dead cells were scattered among an increasing number of green fluorescent live cells

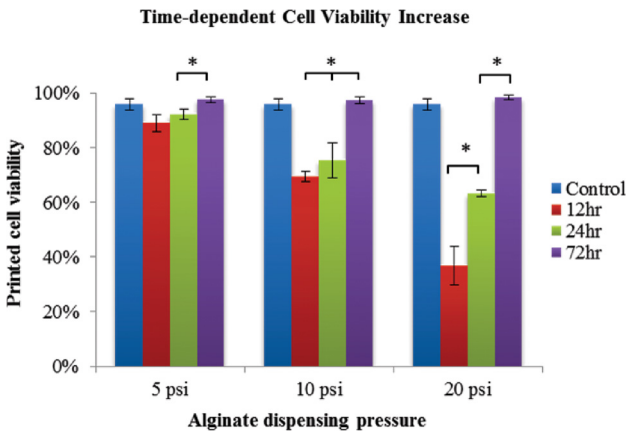

Fig. 10 Cell recovery in the printed structure using $I_{26G}O_{16G}$ during postprinting incubation for a 72 h period. Increased cell viability is observed from 12 h postbioprinting to 72 h incubation at different alginate dispensing pressures (data are mean ± SD; $p < 0.05$).

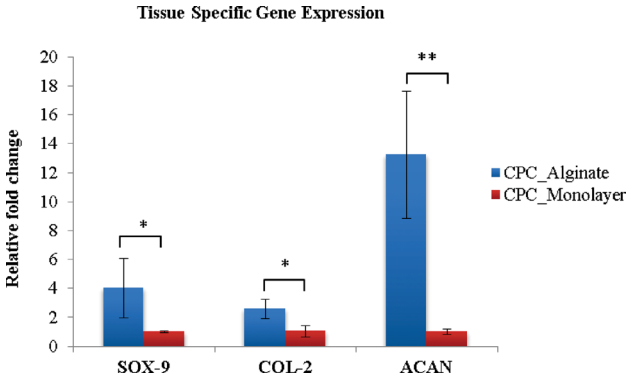

Fig. 11 Real-time PCR revealed significantly higher expression of cartilage-specific markers; PRG-4, Sox-9, and COL-2 all showed over a twofold upregulation in alginate tubular channel encapsulated CPCs compared with CPCs in the monolayer culture after bioprinting. ACAN showed over a 12-fold higher expression level (data are mean ± SD; (*: $p < 0.05$; **: $p < 0.01$)).

Further exploration into the external stimuli generated by the printing system, biomaterial solution, and cell-biomaterial interaction was performed to assess the effect on cells at different spatial and temporal levels during and after bioprinting. In the presented system, the cells were impacted by biomaterial rheological properties, dispensing pressure, crosslinking solution concentration dispensing speed, coaxial nozzle size, and cell seeding density.

Our results suggest that the effects of four parameters studied here—cell density, alginate concentration, alginate dispensing pressure, and coaxial nozzle size—on cell viability were not equal. There was no significant change in cell viability when varying cell seeding density from 2×10^6/ml to 8×10^6/ml, while a noticeable drop of cell viability, from 89% to 31%, was observed when increasing the alginate concentration from 2% to 6%. This may suggest that alteration in biomaterial rheological properties has more impact than cellular interaction on cell damage during the bioprinting process. Increased alginate concentration resulted in higher viscosity, which might generate higher shear stress inside the nozzle, especially at the interface between the nozzle and the biomaterial, causing more cell death.

For two dispensing parameters, alginate dispensing pressure and coaxial nozzle size, viability studies were carried out in a time-dependent manner. Within 12 h after bioprinting, the average cell viability significantly decreases with increased alginate dispensing pressure and smaller coaxial nozzle (the lowest viability was 36% at 20 psi (138 kPa) by $I_{23G}O_{16G}$). This initial cell damage is likely induced by mechanical stresses generated by the shear at the nozzle wall. As shown in Fig. 12, cell viability decrease dramatically as the maximum shear stress increase. In the proposed coaxial nozzle system, there exist two interfaces between the cellular material and the nozzle wall, which further increases the possibility of shear-stress-induced cell damage compared to a single nozzle printing system. As presented in Figs. 6 and 9(*a*), most of the dead cells were distributed along the edge of the walls of printed structures, where shear stresses were the highest. The percentage of dead cells in Fig. 6 is different at both interfaces (outer and inner nozzle interface). Furthermore, increased cell viability at the 24 h and 72 h time points (see Fig. 7) may indicate that damaged cells are able to recover from their compromised status during postprinting incubation. A remarkable increase in cell numbers (see Fig. 7(*a*)) and cell viability 72 h after bioprinting with higher dispensing pressures (10 psi (69 kPa) and 20 psi (138 kPa)) suggests that cells may actually undergo reversible damage rather than permanent cell death, and that many of them were able to proliferate during *in vitro* culture. This observation

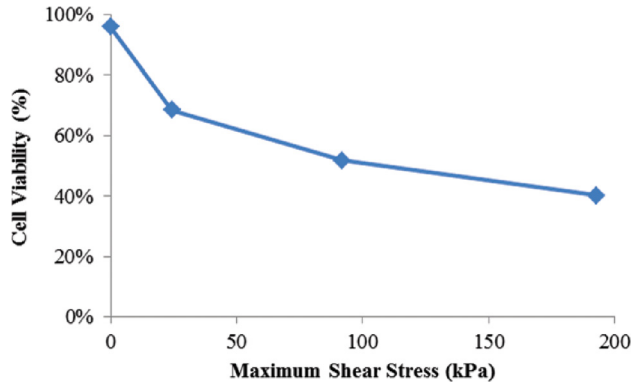

Fig. 12 Cell viability under varying maximum shear stress

may also suggest a potential advantage of the tubular channel structure, which is able to support culture media transportation and provide superior gas exchange within alginate hydrogel.

Moreover, the high expression level of the cartilage-specific genes Col-2, ACAN, and Sox-9 in the printed tubular structure confirmed that progenitor cell function was not altered by our bioprinting system. Instead, CPCs were more likely to differentiate towards their desired lineage, carrying out their ECM-producing function in a printed 3D tubular structure rather than culturing them in a Petri dish.

Although promising results demonstrated the advantages of our system, several limitations have to be recognized in this study. First, the size of fabricated tubular channels was associated with coaxial nozzle assembly capability, which is not able to reach submicron scale by current fabrication techniques. A more sophisticated nozzle assembly as well as deposition system is needed to further fabricate a submicron or even nanoscale tubular structure. Moreover, whether the proposed system is able to process other material with a different gelation mechanism awaits further investigation. Similarly, crosslinking solution could be introduced through the inner section of the coaxial nozzle for crosslinking-based polymerization (i.e., chitosan as in our recent work [38]), while a temperature control unit might be able to be integrated with a coaxial nozzle system to print thermo-sensitive hydrogels such as collagen, agarose, gelatin, etc., by which cold water can be extruded through the core section to initiate polymerization. Furthermore, studies should be made to investigate viability and functionality of vascular cells upon encapsulation and incubation to obtain more convincing data for proposed vascular system bioprinting.

5 Conclusion

This study evaluated the proposed coaxial bioprinting platform for cell-laden tubular channel fabrication, where its manufacturing capacity and, more importantly, biocompatibility were validated. Findings of this research can help with optimization and modification of bioprinting parameters as well as postprinting incubation for future functional three-dimensional organ fabrication and maturation.

Future studies will take advantage of the unique tubular structure to fabricate blood vessels with endothelial cells and smooth muscle cells using a concentric triaxial nozzle assembly, where the introduced coaxial nozzle will be placed in a third nozzle. This setup will enable enclosing the endothelial cell layer with a smooth muscle cell layer printed through the outermost nozzle mimicking the architecture of natural blood vessels. The proposed tubular channels have great promise in printing small-scale, long, and mechanically integrated blood-vessellike channels for future application. Further, a printed vascular system will be integrated with printed tissue spheroids from various cell types like pancreatic cells, hepatocytes, cardiomyocytes, etc., for engineering functioning organs.

Acknowledgment

This research has been supported by the National Institutes of Health (NIH) and the Institute for Clinical and Translational Science (ICTS) grant number ULIRR024979. The authors also would like to thank Mr. John Bierman for his expertise and help in confocal imaging.

References

[1] Langer, R., and Vacanti, J. P., 1993, "Tissue Engineering," Science, **260**(5110), pp. 920–926.
[2] Tang, Q. O., Carasco, C. F., Gamie, Z., Korres, N., Mantalaris, A., and Tsiridis, E., 2012, "Preclinical and Clinical Data for the Use of Mesenchymal Stem Cells in Articular Cartilage Tissue Engineering," Expert Opin. Biol. Thera., **12**(10), pp. 1361–1382.
[3] Griffith, L. G., and Swartz, M. A., 2006, "Capturing Complex 3D Tissue Physiology In Vitro," Nat. Review, **7**(3), pp. 211–224.
[4] Langer, R. S., and Vacanti, J. P., 1999, "Tissue Engineering: The Challenges Ahead," Sci. Am., **280**(4), pp. 86–89.
[5] Mironov, V., Trusk, T., Kasyanov, V., Little, S., Swaja, R., and Markwald, R., 2009, "Biofabrication: A 21st Century Manufacturing Paradigm," Biofabrication, **1**(2), p. 022001.
[6] Boland, T., Xu, T., Damon, B., and Cui, X., 2006, "Application of Inkjet Printing to Tissue Engineering," Biotech. J., **1**(9), pp. 910–917.
[7] Cohen, D. L., Malone, E., Lipson, H., and Bonassar, L. J., 2006, "Direct Free-form Fabrication of Seeded Hydrogels in Arbitrary Geometries," Tissue Eng., **12**(5), pp. 1325–1335.
[8] Wang, X., Yan, Y., Pan, Y., Xiong, Z., Liu, H., Cheng, J., Liu, F., Lin, F., Wu, R., Zhang, R., and Lu, Q., 2006, "Generation of Three-Dimensional Hepatocyte/Gelatin Structures With Rapid Prototyping System," Tissue Eng., **12**(1), pp. 83–90.
[9] Boland, T., Mironov, V., Gutowska, A., Roth, E. A., and Markwald, R. R., 2003, "Cell and Organ Printing 2: Fusion of Cell Aggregates in Three-Dimensional Gels," Anat. Red. A, **272**(2), pp. 497–502.
[10] Xu, T., Jin, J., Gregory, C., Hickman, J. J., and Boland, T., 2005, "Inkjet Printing of Viable Mammalian Cells," Biomaterials, **26**(1), pp. 93–99.
[11] Xu, T., Gregory, C. A., Molnar, P., Cui, X., Jalota, S., Bhaduri, S. B., and Boland, T., 2006, "Viability and Electrophysiology of Neural Cell Structures Generated by the Inkjet Printing Method," Biomaterials, **27**(19), pp. 3580–3588.
[12] Barron, J. A., Wu, P., Ladouceur, H. D., and Ringeisen, B. R., 2004, "Biological Laser Printing: A Novel Technique for Creating Heterogeneous 3-Dimensional Cell Patterns," Biomed. Microdevices, **6**(2), pp. 139–147.
[13] Ringeisen, B. R., Kim, H., Barron, J. A., Krizman, D. B., Chrisey, D. B., Jackman, S., Auyeung, R. Y., and Spargo, B. J., 2004, "Laser Printing of Pluripotent Embryonal Carcinoma Cells," Tissue Eng., **10**(3–4), pp. 483–491.
[14] Odde, D. J., and Renn, M. J., 1999, "Laser-Guided Direct Writing for Applications in Biotechnology," Trends Biotech., **17**(10), pp. 385–389.
[15] Barron, J. A., Ringeisen, B. R., Kim, H., Spargo, B. J., and Chrisey, D. B., 2004, "Application of Laser Printing to Mammalian Cells," Thin Solid Films, **453-454**, pp. 383–387.
[16] Wu, P. K., Ringeisen, B. R., Callahan, J., Brooks, M., Bubb, D. M., Wu, H. D., Piqué, A., Spargo, B., McGill, R. A., and Chrisey, D. B., 2001, "The Deposition, Structure, Pattern Deposition, and Activity of Biomaterial Thin-Films by Matrix-Assisted Pulsed-Laser Evaporation (MAPLE) and MAPLE Direct Write," Thin Solid Films, **398-399**, pp. 607–614.
[17] Khalil, S., and Sun, W., 2007, "Biopolymer Deposition for Freeform Fabrication of Hydrogel Tissue Constructs," Mater. Sci. Eng. C, **27**(3), pp. 469–478.
[18] Ang, T. H., Sultana, F. S. A., Hutmacher, D. W., Wong, Y. S., Fuh, J. Y. H., Mo, X. M., Loh, H. T., Burdet, E., and Teoh, S. H., 2002, "Fabrication of 3D Chitosan–Hydroxyapatite Scaffolds Using a Robotic Dispensing System," Mater. Sci. Eng. C, **20**(1–2), pp. 35–42.
[19] Yan, Y., Xiong, Z., Hu, Y., Wang, S., Zhang, R., and Zhang, C., 2003, "Layered Manufacturing of Tissue Engineering Scaffolds via Multi-Nozzle Deposition," Mater. Lett., **57**(18), pp. 2623–2628.
[20] Melchels, F. P. W., Domingos, M. A. N., Klein, T. J., Malda, J., Bartolo, P. J., and Hutmacher, D. W., 2012, "Additive Manufacturing of Tissues and Organs," Prog. Polym. Sci., **37**(8), pp. 1079–1104.
[21] Mironov, V., Visconti, R. P., Kasyanov, V., Forgacs, G., Drake, C. J., and Markwald, R. R., 2009, "Organ Printing: Tissue Spheroids as Building Blocks," Biomaterials, **30**(12), pp. 2164–2174.
[22] Ozbolat, I., and Yu, Y., 2013, "Bioprinting Towards Organ Fabrication: Challenges and Future Trends," IEEE Trans. Biomed. Eng., **60**(3), pp. 691–699.
[23] Xu, C., Chai, W., Huang, Y., and Markwald, R. R., 2012, "Scaffold-Free Inkjet Printing of Three-Dimensional Zigzag Cellular Tubes," Biotech. Bioeng., **109**(12), pp. 3152–3160.
[24] Ozawa, F., Ino, K., Takahashi, Y., Shiku, H., and Matsue, T., 2013, "Electrodeposition of Alginate Gels for Construction of Vascular-Like Structures," J. Biosci. Bioeng., **115**(4), pp. 459–461.
[25] Napolitano, A., Dean, D., Man, A., Youssef, J., Ho, D., Rago, A., Lech, M., and Morgan, J., 2007, "Scaffold-Free Three-Dimensional Cell Culture Utilizing Micromolded Nonadhesive Hydrogels," BioTechniques, **43**(4), pp. 494–500.

[26] Chang, R., Nam, J., and Sun, W., 2008, "Effects of Dispensing Pressure and Nozzle Diameter on Cell Survival From Solid Freeform Fabrication-Based Direct Cell Writing," Tissue Eng. A, **14**(1), pp. 41–48.
[27] Lin, Y., Huang, Y., Wang, G., Tzeng, T.-R. J., and Chrisey, D. B., 2009, "Effect of Laser Fluence on Yeast Cell Viability in Laser-Assisted Cell Transfer," J. Appl. Phys., **106**(4), pp. 043106–043107.
[28] Cui, X., Dean, D., Ruggeri, Z. M., and Boland, T., 2010, "Cell Damage Evaluation of Thermal Inkjet Printed Chinese Hamster Ovary Cells," Biotech. Bioeng., **106**(6), pp. 963–969.
[29] Nair, K., Gandhi, M., Khalil, S., Yan, K. C., Marcolongo, M., Barbee, K., and Sun, W., 2009, "Characterization of Cell Viability During Bioprinting Processes," Biotech. J., **4**(8), pp. 1168–1177.
[30] Norotte, C., Marga, F. S., Niklason, L. E., and Forgacs, G., 2009, "Scaffold-Free Vascular Tissue Engineering Using Bioprinting," Biomaterials, **30**(30), pp. 5910–5917.
[31] Cui, X., Breitenkamp, K., Finn, M. G., Lotz, M., and D'Lima, D. D., 2012, "Direct Human Cartilage Repair Using Three-Dimensional Bioprinting Technology," Tissue Eng. A, **18**(11–12), pp. 1304–1312.
[32] Duan, B., Hockaday, L. A., Kang, K. H., and Butcher, J. T., 2012, "3D Bioprinting of Heterogeneous Aortic Valve Conduits With Alginate/Gelatin Hydrogels," J. Biomed. Mater. Res. A., **101**(5), pp. 1255–1264.
[33] Yu, Y., 2012, "Identification and Characterization of Cartilage Progenitor Cells by Single Cell Sorting and Cloning," Master's thesis, University of Iowa, Iowa City, IA.
[34] Xiang, L., Wang, S., and Yu, M., 2012, "Alginate Microencapsulation Technology for the Percutaneous Delivery of Adipose-Derived Stem Cells," Ann. Plastic Surg., **68**(2), pp. 229–230.
[35] Chhabra, R. P., and Richardson, J. F., 2008, *Non-Newtonian Flow and Applied Rheology*, Elsevier, Amsterdam.
[36] Zhang, Y., Yu, Y., Chen, H., and Ozbolat, I. T., 2013, "Characterization of Printable Cellular Micro-Fluidic Channels for Tissue Engineering," Biofabrication, **5**(2), p. 025004.
[37] Norton, I. T., Spyropoulos, F., and Cox, P., 2011, *Practical Food Rheology an Interpretive Approach*, Wiley-Blackwell, Oxford.
[38] Zhang, Y., Yu, Y., and Ozbolat, I. T., 2013, "Direct Bioprinting of Vessel-Like Tubular Microfluidic Channels," ASME J. Nanotech. Eng. Med. (in press).